Prime editing for functional repair in patient-derived disease models

Imre F. Schene[1,2,3], Indi P. Joore[2,3]*, Michal Mokry[1], Anke H.M. van Vugt[1,3], Peter M. van Hasselt[2], Edward E.S. Nieuwenhuis[1,4], Sabine A. Fuchs[1,2,5]*

1. Division of Pediatric Gastroenterology, Wilhelmina Children's Hospital, University Medical Center Utrecht, Lundlaan 6, 3584 EA Utrecht, the Netherlands.

2. Department of Metabolic Diseases, Wilhelmina Children's Hospital, University Medical Center Utrecht, Lundlaan 6, 3584 EA Utrecht, the Netherlands.

3. Regenerative Medicine Center Utrecht, Uppsalalaan 8, 3584 CT Utrecht, the Netherlands.

4. Department of Sciences, University College Roosevelt, Lange Noordstraat 1, 4331 CB Middelburg, the Netherlands.

5. Lead Contact, on behalf of 'United for Metabolic Diseases', The Netherlands.

**These authors contributed equally*

Abstract

Prime editing is a novel genome editing technology using fusion proteins of Cas9-nickase and reverse transcriptase, that holds promise to correct a wide variety of genetic defects. We succeeded in efficient prime editing and functional recovery of disease-causing mutations in patient-derived liver and intestinal stem cell organoids.

Main

The development of gene-editing therapies to treat monogenic diseases has long been an essential goal of CRISPR/Cas9 research. Cas9-mediated homology-directed repair (HDR) can create all desired base substitutions, insertions and deletions (indels). However, HDR relies on introduction of double-stranded DNA breaks, is inefficient and error-prone[1,2]. Base editing, that uses Cas9-nickases fused to DNA-modifying enzymes, is more efficient and accurate than HDR, but can only correct four out of twelve point mutations and no small insertions and deletions. Furthermore, base editing requires a suitable protospacer adjacent motif (PAM) and the absence of co-editable nucleotides[3].

Prime editing combines a nicking-Cas9–reverse transcriptase fusion protein (PE2) with a prime editing guide RNA (pegRNA) containing the desired edit. The pegRNA-spacer guides the formation of a nick in the targeted DNA strand. The pegRNA-extension binds to this nicked strand and instructs the synthesis of an edited DNA flap. This edited flap is then integrated by DNA repair mechanisms, which can be enhanced by simultaneous nicking of the non-edited strand (Supplementary Fig. 1)[4].

Prime editing has been applied in human cancer cell lines and plant cells, but not in human disease models[4,5,6]. Adult stem cell-derived organoids exhibit important functional properties of organs, allowing modeling of monogenic diseases[7]. We set out to develop and test prime editing in primary patient-derived organoids.

We first optimized prime editing for organoid cells using deletions and single-nucleotide substitutions previously performed in HEK293T cells[4]. The non-edited strand was nicked by a second 'nicking sgRNA' to enhance editing (PE3). Our optimized protocol consisted of co-transfection of prime edit plasmids with a GFP-reporter plasmid allowing selection and subsequent clonal expansion of transfected cells. Prime editing of intestinal and ductal liver organoids resulted in efficient (>50%) deletion of 5 nucleotides in *HEK3* (Fig. 1b and Supplementary Fig. 2). Furthermore, we were able to induce a transversion mutation located 26 nucleotides downstream of the nick with substantial efficiency (20%) (Fig. 1c). These results show successful prime editing of primary stem cells with similar efficiency as observed in human cancer cell lines.

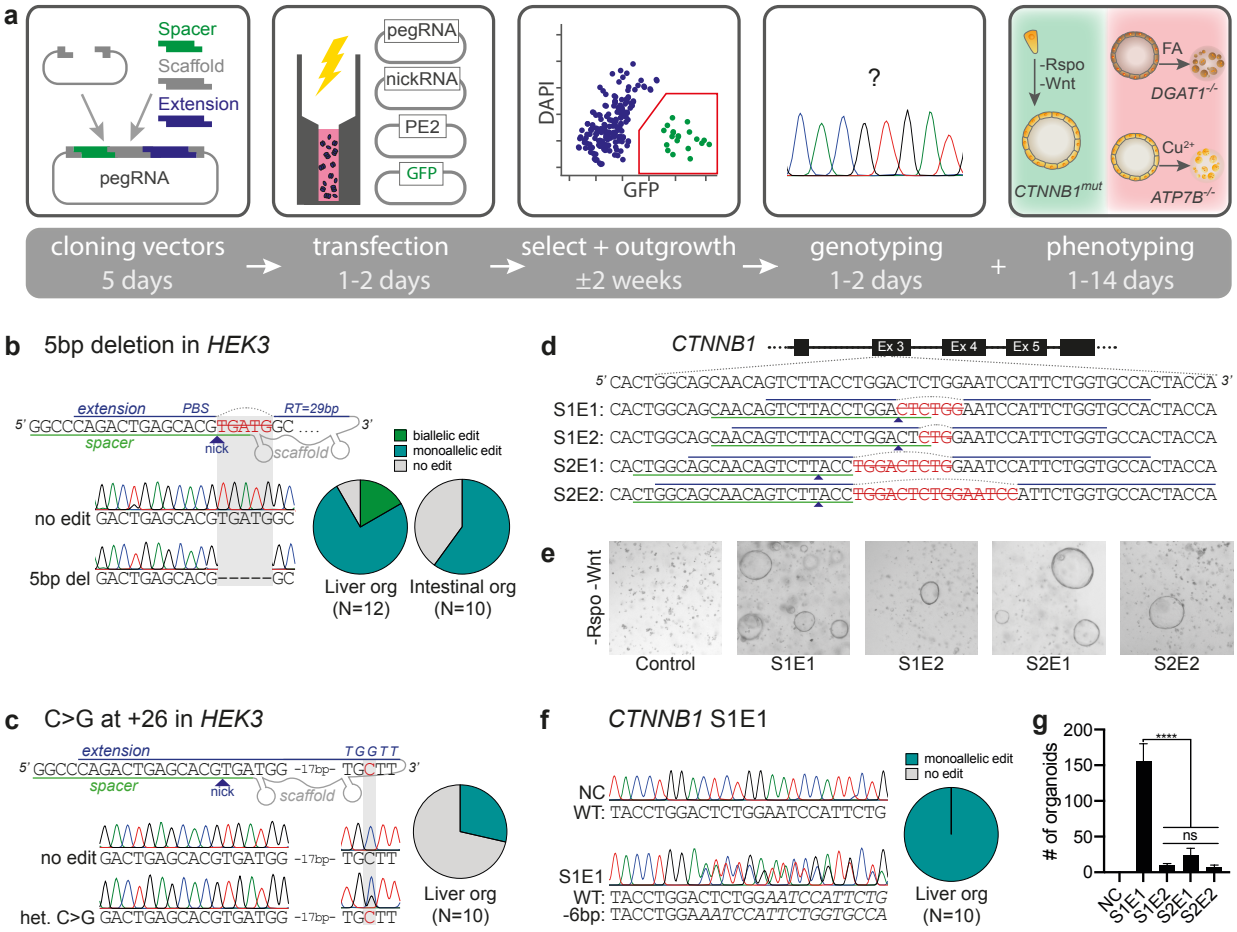

Figure 1: Prime editing efficiently creates deletions and point mutations in stem cells

a, Schematic overview of the workflow and timeline to generate precise mutations in organoid cells using prime editing (PE3). **b**, pegRNA design, Sanger validation, and editing efficiency of a 5-bp deletion in *HEK3* in liver and intestinal organoids. **c**, pegRNA design, Sanger validation, and editing efficiency of a C→G substitution in *HEK3* in liver organoids. Nicking sgRNA at +90 used in **(b)** and **(c)** not shown. **d**, pegRNA designs for the generation of in-frame deletions in the ß-TrCP region of CTNNB1. Nicking sgRNA at +86 (S1) or +93 (S2) not shown. **e**, Brightfield images of liver organoid cells transfected with plasmids from **(d)** and after -Rspo1 conditions for 2 weeks. **f**, Sanger validation of precise 6-bp deletions in all picked clones from *CTNNB1* pegRNA S1E1. **g**, Quantification of organoid outgrowth in **(e)**. Error bars represent S.E.M. of three independent experiments.

48 Next, we targeted the Wnt-pathway intermediate ß-catenin (*CTNNB1*) in organoids. Activating
49 carcinogenic *CTNNB1* mutations are found in ±40% of hepatocellular carcinoma, resulting in Wnt-
50 signaling independent of exogenous stimuli[8]. We designed PE3 plasmids, containing pegRNA-
51 extensions with primer binding sites (PBSs) and RT-templates of various lengths, that all create in-
52 frame deletions in the ß-TrCP region required for CTNNB1 ubiquitination (Fig. 1d). As wildtype liver
53 organoid expansion depends on Wnt-pathway activation, edited cells could be selected by
54 withdrawing Wnt-agonist R-spondin 1 (Fig. 1e). Sequencing confirmed that all clones grown without
55 R-spondin for two weeks contained heterozygous in-frame deletions in *CTNNB1* (Fig. 1f and
56 Supplementary Fig. 2c). We observed striking differences (up to a factor 50) in editing efficiencies of
57 different pegRNA designs (Fig. 1g). Next, we generated the severe *ABCB11*^{D482G} mutation, a frequent
58 cause of bile salt export pump (BSEP) deficiency[9]. This nucleotide substitution was generated with
59 20% efficiency in liver organoids when silent PAM mutations were introduced (Supplementary Fig. 3).
60 These results demonstrate the utility of prime editing in creating disease models and the importance
61 of testing different pegRNA designs to induce the desired edit.

62 To investigate prime editing for functional correction of disease-causing mutations, we studied
63 *diacylglycerol-acyltransferase 1* (*DGAT1*) in patient-derived intestinal organoids. *DGAT1* encodes an
64 enzyme catalyzing the conversion of diacylglycerol and fatty acyl-CoA to triacylglycerol. When DGAT1
65 function is deficient, fatty acids (FAs) cannot be incorporated in lipid droplets and instead cause
66 lipotoxicity and cell death (Fig. 2a). *DGAT1* mutations result in congenital diarrhea and protein-losing
67 enteropathy upon lipid intake[10]. The common biallelic 3-bp deletion (c.629_631delCCT, p.S210del) in
68 exon 7 of *DGAT1* leads to complete absence of the mature protein (Fig. 2b,e)[10]. We designed PE3
69 plasmids to promote the insertion of the missing three nucleotides. These plasmids were transfected
70 into patient-derived organoid cells and organoids were grown from single transfected cells. Sanger
71 sequencing of clonal organoids revealed repair of the pathogenic deletion (Fig. 2b). To demonstrate
72 DGAT1 function of prime edited cells, we exposed organoids to FAs, which are harmless to healthy
73 control organoids and toxic to DGAT1-deficient organoids (Fig. 2c,d and Supplementary Fig. 4). All
74 clones surviving functional selection were genetically repaired (Fig. 2f), and showed normal DGAT1
75 protein expression (Fig. 2e and Supplementary Fig. 5). Next, we compared prime editing to HDR in
76 terms of efficiency and accuracy. The ratio of correct editing to unwanted indels was ±30-fold higher
77 for prime editing than for Cas9-initiated HDR (Fig. 2f and Supplementary Fig. 5). These findings show
78 that prime editing, as opposed to base editing, can repair small deletions with considerably more
79 precision and efficiency than HDR.
80 To compare prime editing to base editing, we selected two severe pathogenic G→A mutations
81 suitable for correction by adenine base editors (ABEs): the BSEP-deficiency mutation *ABCB11*^{R1153H}
82 and the alpha-1 antitrypsin deficiency ZZ-genotype (*SERPINA1*^{E342K})[9,11]. Base editing outperformed
83 prime editing in efficiency (Supplementary Fig. 6), indicating that the added value of prime editing
84 currently lies in correcting mutations that are uneditable by base editors.

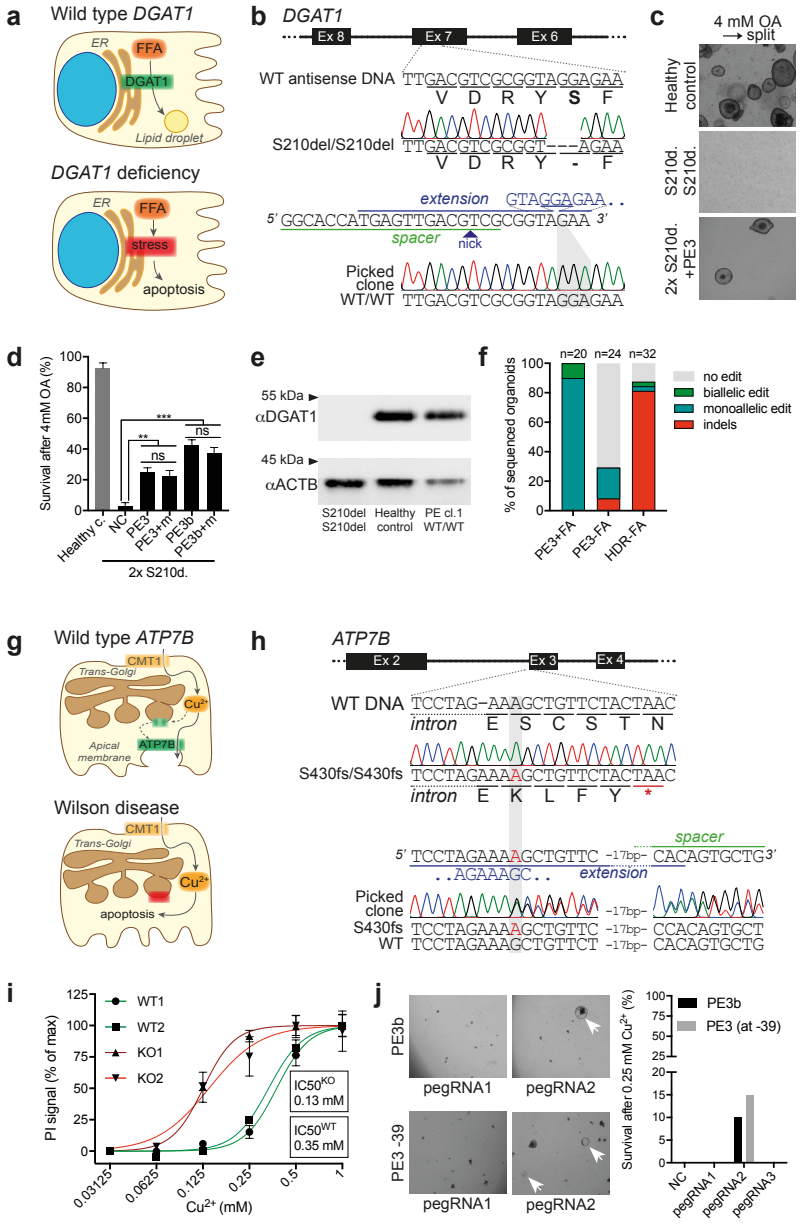

Figure 2: Prime editing functionally corrects disease-causing indel mutations in intestinal and liver organoids. **a**, Schematic overview of the DGAT1 disease mechanism. **b**, Sanger validation of biallelic *DGAT1*^{S210del} mutations in patient-derived intestinal organoids, pegRNA design (nicking sgRNA at +46 not shown), and validation of biallelic correction by PE3. **c**, Brightfield images of healthy control- and *DGAT1* ^{S210del} patient-derived intestinal organoids (±PE3) after exposure to 4 mM oleic acid (OA) for 24h and splitting. **d**, Quantification of organoid survival in **(c)**. **e**, Western blot of DGAT1 in *DGAT1*^{S210del} patient-, PE3-corrected patient-, and healthy control-organoids. **f**, Quantification of intended edit and unwanted indels by PE3 and HDR in *DGAT1*^{S210del} organoids. For PE3, with (+FA) and without (-FA) OA selection was considered. **g**, Schematic overview of the Wilson disease (*ATP7B* deficiency) mechanism. **h**, Sanger validation of biallelic *ATP7B*^{S430fs} mutations in patient-derived liver organoids, pegRNA#2 design, and validation of monoallelic correction by PE3. **i**, Cell death in *ATP7B*^{WT} and ATP7B^{KO} liver organoids after incubation with Cu^{2+} for 3 days. **j**, Representative brightfield images and quantification of Cu^{2+}-survival in *ATP7B*^{S430fs}-patient organoids after PE3 with various pegRNAs. White arrowheads indicate surviving organoids.

85 Next, we set out to repair a 1-bp duplication (c.1288dup, p.S430fs) in *ATP7B*, causing Wilson disease.
86 *ATP7B* encodes a copper-transporter (ATP7B), facilitating excretion of excess copper into the bile
87 canaliculus (Fig. 2g). Pathological accumulation of copper in the liver of Wilson disease patients leads
88 to liver cirrhosis requiring lifelong treatment and ultimately liver transplantation[12]. We designed
89 several PE3 conditions to remove the 1-bp duplication in patient-derived liver organoids
90 (Supplementary Fig. 8). Clonal picking of transfected organoid cells confirmed monoallelic repair of
91 the disease-causing mutation by pegRNA#2 (Fig. 2h). We then generated *ATP7B*^{KO} organoids that
92 were more susceptible to copper-induced cell death than *ATP7B*^{WT} organoids (Fig. 2i and
93 Supplementary Fig. 7).
94 To demonstrate functional repair of *ATP7B*^{S430fs} organoids after prime editing, transfected cells were
95 exposed to copper for 4 days (Supplementary Fig. 2). Out of three different pegRNA plasmids, only
96 successful monoallelic repair with pegRNA#2 resulted in rescue of copper excretion (Fig. 2j). These
97 results confirm the ability of prime editing to genetically and functionally correct truncating
98 mutations and underline the importance of testing various pegRNA designs.
99
100 Versatile and efficient gene editing in primary cells would represent a gamechanger for both in vitro
101 modeling of monogenetic disease and treatment with autologous gene-corrected cells. We here
102 provide a protocol for prime editing in human adult stem cells. Using this protocol, we demonstrate
103 that prime editing can generate insertions, deletions, and various point mutations and functionally
104 correct disease phenotypes in patient-derived stem cells. Importantly, prime editing results in higher
105 efficiency and drastically lower indel-formation compared to Cas9-mediated HDR. In the subset of
106 mutations applicable to base editing, prime editors are currently less robust than the latest
107 generation of base editors.
108
109 Our data in primary adult stem cells corroborate findings in cancer cell lines, in which prime editing
110 typically offers greater precision than Cas9-mediated HDR and lower on-target efficiency than base
111 editing, when the target nucleotide is suitably located[4]. Base editing, however, has been subject to
112 various stages of optimization, whereas prime editing is still in its infancy[11,13,14]. The efficiency of
113 prime editing in mammalian and plant cells has been strongly associated with pegRNA design, but
114 optimal PBS and RT-template parameters remain elusive and differ between target sites[4,6]. In our
115 hands, pegRNA design also had profound effects on editing efficiency, with PBS lengths of 10-12
116 nucleotides outperforming longer designs (Figures 1G and 2J). We expect that pegRNA design as well
117 as the prime editor fusion protein can be further optimized to improve prime editing efficiency in the
118 future.

119 To conclude, this study confirms the potential of prime editing to model and repair human
120 monogenic diseases and represents an important first step towards future clinical application.

121 **References**

122 1. Chapman, J. R., Taylor, M. R. G. & Boulton, S. J. Playing the End Game: DNA Double-
123 Strand Break Repair Pathway Choice. *Mol. Cell* **47**, 497–510 (2012).
124 2. Paquet, D. *et al.* Efficient introduction of specific homozygous and heterozygous
125 mutations using CRISPR/Cas9. *Nature* **533**, 125–129 (2016).
126 3. Rees, H. A. & Liu, D. R. Base editing: precision chemistry on the genome and
127 transcriptome of living cells. *Nat. Rev. Genet.* **19**, 770–788 (2018).
128 4. Anzalone, A. V. *et al.* Search-and-replace genome editing without double-strand breaks
129 or donor DNA. *Nature* **576**, 149–157 (2019).
130 5. Xu, R. *et al.* Development of a plant prime editing system for precise editing in the rice
131 genome. *PLANT Commun.* 100043 (2020). doi:10.1016/j.xplc.2020.100043
132 6. Lin, Q. *et al.* Prime genome editing in rice and wheat. *Nat. Biotechnol.* (2020).
133 doi:10.1038/s41587-020-0455-x
134 7. Clevers, H. Modeling Development and Disease with Organoids. *Cell* **165**, 1586–1597
135 (2016).
136 8. Rebouissou, S. *et al.* Genotype-phenotype correlation of CTNNB1 mutations reveals
137 different ß-catenin activity associated with liver tumor progression. *Hepatology* **64**,
138 2047–2061 (2016).
139 9. Strautnieks, S. S. *et al.* Severe Bile Salt Export Pump Deficiency: 82 Different ABCB11
140 Mutations in 109 Families. *Gastroenterology* **134**, 1203–1214 (2008).
141 10. van Rijn, J. M. et al. Intestinal Failure and Aberrant Lipid Metabolism in Patients With
142 DGAT1 Deficiency. Gastroenterology 155, 130-143.e15 (2018).
143 11. Huang, T. P. *et al.* Circularly permuted and PAM-modified Cas9 variants broaden the
144 targeting scope of base editors. *Nat. Biotechnol.* **37**, 626–631 (2019).
145 12. Członkowska, A. *et al.* Wilson disease. *Nat. Rev. Dis. Prim.* **4**, 1–20 (2018).
146 13. Koblan, L.W. *et al.* Improving cytidine and adenine base editors by expression
147 optimization and ancestral reconstruction. *Nat Biotechnol.* **36**, 843-846 (2018).
148 14. Miller, S.M., *et al.* Continuous evolution of SpCas9 variants compatible with non-G
149 PAMs. *Nat. Biotechnol.* **38**, 471–481 (2020).

150 **Methods**

151

152 **Study approval and human subjects**

153 The study was approved by the responsible local ethics committee (Institutional Review Board of the
154 University Medical Center Utrecht).

155

156 **Organoid culture**

157 Liver and intestinal organoids were cultured and passaged according to previously described
158 protocols[13,14]. After thawing, organoids were passaged at least once before electroporation.

159

160 **Plasmid cloning**

161 Cloning of pegRNA plasmids was performed according to previously described protocols[4]. For cloning
162 of sgRNAs used for PE3 and ABE-NG, we replaced the BsmBI restriction sites of the sgRNA expression
163 vector BPK1520 by BbsI restriction sites using PCR, which allowed direct ligation of sgRNA-spacer
164 duplexes according to a previously described method[15]. All pegRNA, sgRNA, HDR template, and
165 primers sequences used in this work are listed in Supplementary Tables 1–3 and were synthesized by
166 Integrated DNA Technologies (IDT). pCMV-PE2 (Addgene #132775), pU6-pegRNA-GG-acceptor
167 (Addgene #132777), and NG-ABEmax (Addgene #124163) were gifts from David Liu; BPK1520
168 (Addgene #65777) was a gift from Keith Joung; pSpCas9(BB)-2A-Puro (PX459, Addgene #62988) was a
169 gift from Feng Zhang.

170

171 **Electroporation**

172 Before electroporation, organoids were grown under normal conditions in 30 µl Matrigel per well.
173 Two days prior to electroporation, organoids were cultured in medium containing surrogate WNT
174 protein (4 nM). Four wells containing organoids were then dissociated for each condition using
175 TrypLE for 4-5 minutes at 37°C and applying mechanical disruption through pipetting. Cells were
176 washed once using Advanced DMEM/F12, resuspended in 80 µl OptiMEM containing Y-27632 (10
177 µM), and 20 µl DNA mixture was added. For prime editing, the DNA mixture contained 12 µg PE2
178 plasmid, 5 µg pegRNA plasmid, 2 µg nicking sgRNA plasmid, and 1 µg GFP plasmid. For HDR, the DNA
179 mixture contained 15 µg sgRNA containing-Cas9 plasmid (PX459), 1 µl of 100 µM HDR template, and
180 1 µg GFP plasmid. For base editing, the DNA mixture contained 15 µg NG-ABEmax plasmid, 4 µg
181 sgRNA plasmid, and 1 µg GFP plasmid. For generation of *ATP7B* knockout organoids, the DNA mixture
182 contained 15 µg sgRNA containing-Cas9 plasmid (PX459) and 1 µg GFP plasmid. The cell-DNA mixture
183 was transferred to an electroporation cuvette and electroporated using settings described before[16].
184 Cells were removed from the cuvette and transferred into 500 µl OptiMEM containing Y-27632 (10

185 µM). After 20 minutes, cells were plated in 180 µl matrigel. Upon polymerization of the Matrigel,
186 medium was added containing surrogate WNT protein (4 nM) and Y-27632 (10 µM).
187
188 **FACS**
189 2-3 days after electroporation using the GFP plasmid, cells were dissociated with TrypLE for 2-3
190 minutes at 37°C. The cells were washed once using Advanced DMEM/F12 and resuspended in 400 µl
191 FACS buffer (PBS with 2 mM EDTA and 0.5% BSA). FACS was used to filter the GFP+ cell population,
192 selecting specifically for transfected cells (FACS Aria, BD). GFP+ cells were retrieved in medium
193 containing surrogate WNT protein (4 nM) and Y-27632 (10 µM), after which the cells were plated as
194 soon as possible at a cell-concentration of 300 cells per 30 µl Matrigel. Upon polymerization of the
195 Matrigel, medium was added containing surrogate WNT protein (4 nM) and Y-27632 (10 µM).
196
197 **Genotyping**
198 Single organoids were picked using a p200 pipette and dissociated using TrypLE for 2-3 minutes at
199 37°C. Cells were resuspended in 30 µl Matrigel total of which 20 µl was plated. DNA was extracted
200 from the remaining 10 µl Matrigel using the Zymogen Quick-DNA microprep kit according to
201 manufacturer instructions. Q5 high fidelity polymerase was used to amplify the genomic region of
202 interest. The PCR product was purified using the Qiagen PCR clean-up kit according to manufacturer
203 instructions. Resulting product was sent for sequencing to the Macrogen Europe service EZSeq.
204
205 **Protein blotting**
206 Organoids were lysed in Laemmli buffer (0.12 M Tris HCl pH 6.8, 4% SDS, 20% glycerol, 0.05 g/l
207 bromophenol blue, 35 mM β-mercaptoethanol). Protein concentration was measured using a BCA
208 assay. For western blotting, equal amounts of protein were separated by SDS-PAGE on a 10%
209 acrylamide gel and transferred to PVDF membranes using a Trans-Blot® Turbo machine (Bio-rad)
210 according to manufacturer's protocol. For dot blotting, protein was directly loaded on PVDF
211 membranes without SDS-PAGE separation. The membrane was blocked with 5% milk protein in TBST
212 (0.3% Tween, 10 mM Tris-HCl pH 8 and 150 mM NaCl in distilled water) and probed with primary
213 antibodies against DGAT1 (ab181180; 1:000; Abcam) or ACTB (sc-47778; 1:5000, Santa Cruz
214 Biotechnology) overnight at 4°C. After incubation with HRP-conjugated secondary antibodies
215 (1:5000, Sigma, 1h at RT), bands or dots were imaged on a chemiluminescence detection system
216 (Bio-rad).

217 **Functional assays**

218 To select liver organoids with in-frame mutations in *CTNNB1*, organoids were cultured in normal
219 culture medium without R-spondin 1 for two weeks. To test DGAT1 function in intestinal organoids,
220 oleic acid was added to the culture medium for 24h as previously described[10], and organoid survival
221 was assessed by visual inspection and survival after passaging. To test ATP7B function in liver
222 organoids, copper(II)chloride ($CuCl_2$) was added to the culture medium for 3-4 days. Cell death was
223 quantified by addition of propidium iodide (PI) (0.1 mg/mL, ThermoFisher) to the culture medium for
224 15 minutes. Organoids were imaged by an inverted Olympus IX53 epifluorescence microscope. PI
225 signal was quantified using ImageJ and normalized to a positive control condition for cell death (1
226 mM $CuCl_2$). Based on *ATP7B*^{KO} lines, prolonged organoid survival in 0.25 mM $CuCl_2$ was considered as
227 a characteristic of functional ATP7B.

228

229 **Statistics and reproducibility**

230 No pre-specified effect size was calculated, and no statistical method was used to predetermine
231 sample size. For comparisons of multiple groups, an ordinary one-way ANOVA with Holm–Sidak
232 correction for multiple comparisons was used. In Fig. 1g and Fig. 2d the negative control and the
233 healthy control, respectively, were excluded from statistical comparisons. Statistical tests were
234 appropriate for comparisons being made; assessment of variation was carried out but not included.
235 Experiments were not randomized. Investigators were not blinded to allocation during experiments
236 but outcome assessment (sequencing and functional assay quantification) were performed blinded.
237 Reproducibility: Fig. 1b representative of 12 and 10 clonal liver and intestinal organoids, respectively,
238 each from two independent transfection experiments. Fig. 1c and Fig. 1f representative of 10 clonal
239 liver organoids, from two and three independent transfection experiments, respectively. Fig. 1g
240 representative of three transfection experiments using the same liver organoid donor. Fig. 2d
241 representative of two transfection experiments. Fig. 2f representative of 20-32 clonal organoids from
242 two independent experiments. Fig. 2i representative of two experiments. Fig. 2j represents a single
243 experiment. Supplementary Fig. 3 representative of 30 clonal liver organoids form two independent
244 experiments. Supplementary Fig. 6a and 6b representative of 10 clonal liver organoids per condition,
245 collected through two independent experiments.

246

247 **Data and code availability**

248 No software, code, or large genomic/expressional datasets are included in the current version of this
249 manuscript. Source data for the figures have been provided as Supplementary Table 4. All other data
250 supporting the findings of this study are available from the corresponding author on reasonable
251 request.

252 **References**

253 15. Sato, T. *et al.* Single Lgr5 stem cells build crypt-villus structures in vitro without a
254 mesenchymal niche. *Nature* **459**, 262–5 (2009).
255 16. Huch, M. *et al.* In vitro expansion of single Lgr5 + liver stem cells induced by Wnt-driven
256 regeneration. *Nature* **494**, 247–250 (2013)
257 17. Ran, F. A. *et al.* Genome engineering using crispr-cas9 system. *Chromosom. Mutagen.*
258 *Second Ed.* **8**, 197–217 (2014).
259 18. Fuji, M. *et al.* Efficient genetic engineering of human intestinal organoids using
260 electroporation. *Nat Protoc* **10**, 1474–85 (2015).
261

262 **Acknowledgements**

263 We thank L. van der Laan (LETIS, Erasmus MC, the Netherlands) for sharing liver organoids derived
264 from a Wilson disease patient. We also thank M. Geurts (Hubrecht Institute, the Netherlands) for
265 providing WNT surrogate and for sharing his experiences with Prime Editing. This work was
266 supported by Metakids funding (to S.A.F.) and a Clinical Fellows grant from The Netherlands
267 Organisation for Health Research and Development Health Institute (40-00703-97-13537 to S.A.F.).
268

269 **Author information**

270 These authors contributed equally: Imre F. Schene and Indi P. Joore.
271

272 Affiliations

273 *Division of Pediatric Gastroenterology, Wilhelmina Children's Hospital, University Medical Center*
274 *Utrecht, Utrecht, the Netherlands*
275 Imre F. Schene, Michal Mokry, Anke H.M. van Vugt, Edward E.S. Nieuwenhuis, Sabine A. Fuchs

276 *Department of Metabolic Diseases, Wilhelmina Children's Hospital, University Medical Center*
277 *Utrecht, Utrecht, the Netherlands*
278 Imre F. Schene, Indi P. Joore, Peter M. van Hasselt, Sabine A. Fuchs.

279 *Regenerative Medicine Center Utrecht, Utrecht, the Netherlands*
280 Imre F. Schene, Indi P. Joore, Anke H.M. van Vugt

281 *Department of Sciences, University College Roosevelt, Middelburg, the Netherlands*
282 Edward E.S. Nieuwenhuis
283

Author Contributions

I.F.S., I.P.J., and S.A.F. designed the project; I.F.S., I.P.J., and A.J.M.v.V. performed the experiments; I.F.S., I.P.J., M.M., P.M.v.H., E.E.S.N., and S.A.F. wrote the manuscript.

Corresponding author

Correspondence to Sabine A. Fuchs.

Ethics declarations

Conflict of interest

Authors declare that they have no conflicts of interest.

Supplementary information

Supplementary Figure 1: Overview of the prime editing-principle

Supplementary Figure 2: Representative FACS plot example and different protocols used in this study

Supplementary Figure 3: Generation of *ABCB11*^{D482G} by prime editing (PE3)

Supplementary Figure 4: Functional correction of *DGAT1*^{S210del} by prime editing (PE3)

Supplementary Figure 5: Prime editing (PE3) and Cas9-mediated HDR to correct *DGAT1*^{S210del}

Supplementary Figure 6: Correction of *ABCB11*^{R1153H} and *SERPINA1*^{E342K} by base editing

Supplementary Figure 7: Validation of a functional assay for ATP7B function

Supplementary Figure 8: PegRNA designs used for correction of ATP7B^{S410fs}

Supplementary Table 1: Sequences of pegRNAs used in this study

Supplementary Table 2: Sequences of sgRNAs and HDR templates used in this study

Supplementary Table 3: Sequences of PCR and sequencing primers used in this study

Supplementary Table 4: Source data for figures